research article

Acoustic monitoring of hydraulic fracture growth

Remco Romijn and Jeroen Groenenboom[1]

Introduction

Hydraulic fracturing is a technique to improve the inflow performance of oil and gas wells by creating large fractures around the borehole. By doing this, a highly permeable path is created through which the hydrocarbons can flow to the well more easily. The process consists of two phases. In the first phase, a suitable fluid is pumped into the reservoir under great pressure, thereby rupturing the formation and creating fractures. In the second phase, a propping agent, usually a well-sorted sand, is added to the fluid, and after injecting this mixture for some time, the pumps are stopped. The remaining fluid in the fracture leaks away and the fracture closes on the proppant, thus providing the highly conductive path aimed for.

The success of fracture treatments depends on our ability to predict and influence the fracture shape and orientation. In the Geometry of Hydraulic Fractures project, sponsored by a consortium of oil and service companies and the Dutch Technology Foundation, the physics of hydraulic fracture growth is being studied. To this end, scaled fracturing experiments are being carried out at the rock-mechanics laboratory at the faculty of Applied Earth Sciences. These hydraulic fracture experiments on model blocks are monitored by an acoustic scanning technique using active transducers.

An artificial rock cube (made of cement or plaster) with edges of 0.3 m, is placed in a compression machine to apply an *in-situ* confining stress. A fracturing fluid is injected through a borehole assembly mounted in the block and eventually a fracture is created inside the block. The fracture grows with a rate of about 0.1 mm s^{-1}. After a certain time the pump is stopped (called *shut-in*) and the fracture is allowed to close again. The total duration of the experiment is in the order of hours. During all stages of fracture initiation, growth and closure, acoustic waves scan the complete block every 30 s. The recording time of a separate *scan* is in the order of one millisecond, so each one can be regarded as a still picture taken of the growing hydraulic fracture. With 48 transducers scanning the entire block, different combinations of sending and receiving transducers or *records*, reveal different aspects of the fracture, e.g. radial extent and width. Because we use both P- and S-waves, different features of the scattering of acoustic waves by fractures can be observed. Some aspects of these measurements have been discussed by Groenenboom & Romijn (1996) and Groenenboom *et al.* (1997a). These laboratory experiments closely resemble seismic monitoring surveys of hydraulic fracturing jobs as performed in the field (Wills *et al.* 1992; Meadows & Winterstein 1994).

Laboratory setup

The laboratory setup used for the hydraulic fracturing experiments and acoustic scanning is shown in Fig. 1; Fig. 2 is a diagram of the acoustic data acquisition system. Full detail of the laboratory setup is given by Weijers (1995) and Savic (1995); it consists of several parts.

- *Tri-axial compression machine*

The tri-axial compression machine consists of three perpendicular compression systems, which can each independently deliver a maximum force of 3500 kN. In this way we can apply an anisotropic stress field to the sample. Since this is an open

Figure 1 Laboratory set-up for a hydraulic fracturing experiment. Visible from left to right are the acoustic data acquisition tower, the injection pump and the tri-axial compression machine with one of its doors removed, so a clear view of the sample position and the loading platens, in which the transducers are mounted, is given.

[1]Delft University of Technology, Faculty of Applied Earth Sciences, Section of Applied Geophysics & Petrophysics, PO Box 5028, 2600 GA Delft, The Netherlands

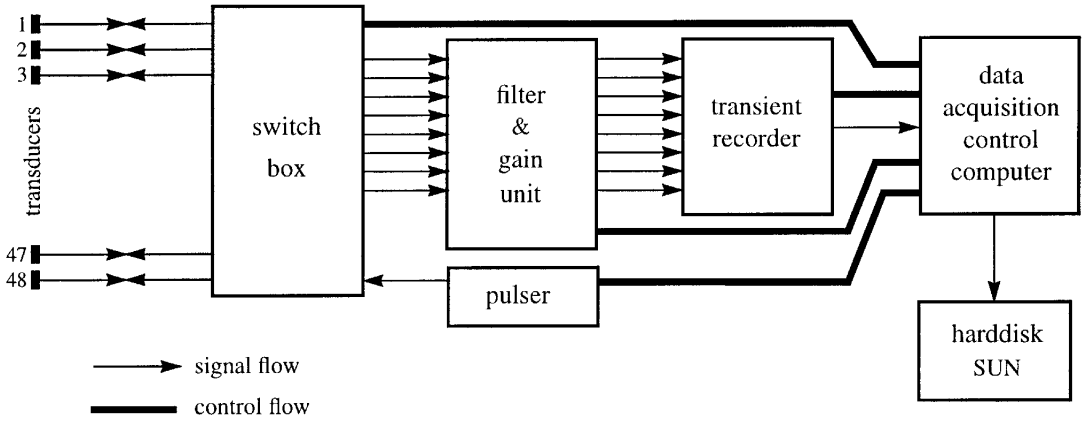

Figure 2 Schematic diagram of the acoustic data acquisition system.

system, it is not possible to apply pore pressure to the rock. With a block of side length 0.30 m, the maximum pressure we can impose is 40 MPa, which corresponds to downhole situations at a depth of about 3000 m. The machine is operated by computer controlled feed-back of the actual force and by measurements of displacements on the outside of the block.

• *Borehole Assembly & Injection System*
In the model blocks, a borehole with a diameter of 23 mm is cast to simulate the well. It can be completed with a casing with various perforation geometries to use in different experiments. Another type of completion, with only one circumferential notch in the borehole wall, positioned in the middle, is used to initiate simple radial fractures. With a linear variable differential transformer (LVDT) fitted inside the borehole, a width measurement of the hydraulic fracture can be obtained. The wellbore is then filled with a fracturing fluid and the fracture is initiated by increasing the fluid pressure using a high pressure pump.

• *Transducers*
The transducers that we use, for generating P-waves and S-waves, are manufactured by Panametrics (models V103-RM and V153-RM). These piezo-electric contact ceramic type transducers generate waveforms with a peak frequency of 1 MHz with a corresponding source signal length of about 2 microsec. The active element size is 13 mm in diameter and overall 16 mm in height. The transducers are mounted in steel loading platens, which allows the tri-axial pressure machine to exert its full pressure to the rock sample, while keeping the transducers *directly* coupled to the block with a constant force of 0.9 kN. Through careful design of these loading platens and by using 0.1 mm-thick sheets of teflon (greased with vaseline), shear stresses acting on the block face are minimized, thus avoiding inhomogeneous stress distributions inside the rock sample.

• *Pulser*
The pulser is the electronic device used to generate the high voltage pulse for driving the source transducers. We use the Panametrics model PR5058. This model can output pulses of up to 900 V, which are necessary to provide the transducers with enough energy to emit acoustic waves with sufficient signal-to-noise ratio.

• *Switchbox*
The switchbox is at the core of the acquisition system. It is custom built and currently can handle up to 48 channels. Its role is to connect the pulser, the transducers and the recording unit in such a way that all channels can operate independently from each other in three modes: the active (transmitting) mode, the passive (receiving) mode and the pulse-echo (transmit-receive) mode. It is designed to be able to transmit a pulse of 900 V and at the same time receive signals from the transducers of only a few millivolts with minimum cross-talk. Every channel contains a preamplifier that boosts the incoming signals from the transducers by 14 dB, prior to passing them through to the *filter & gain unit*.

• *Filter & Gain Unit*
Our custom built 8 channel analogue filter & gain unit is designed to work in conjunction with the switchbox for adequate and versatile signal conditioning prior to A/D conversion. This computer-controlled switchable system allows us to choose from a set of high-pass and low-pass filters the optimal settings for frequency filtering. The low-pass filter is used mainly for antialias filtering, suited to the chosen sampling rate, and the high-pass filter is used to filter out the strong low frequency noise present, which would otherwise quickly saturate the available dynamic range of the A/D converters.

After high-pass filtering, but prior to low-pass filtering, the acoustic signals are subjected to amplification in order to use the full resolution of the A/D converters. Every record (i.e. combination of sending- and receiving transducer pair) has its own tuned gain value. These gains are selected from a fixed set of values, ranging from 2 to 2000, and can be either automatically determined or set by the user.

• *Transient Recorder*
The waveform digitizer & storage device we use is an 8 channel transient recorder from Bakker Electronics (model BE256). This particular model can sample with frequencies ranging from 1 to 10MHz and provides a resolution of 12 bits per word. The dynamic range is therefore 72 dB. The internal buffer memory can hold up to 8 Mb of data. The maximum record length is 8192 samples, the data sample format is 2 byte

integers. Data transfer to the control computer is via a GPIB (IEEE-488) bus, operating at 0.5 Mb s^{-1}.

• *Control Computer & Data Streaming*
The whole data acquisition system is managed by an INTEL-486 based PC, which controls the various parts of the *acoustic tower* and receives the output data from the transient recorder. These raw data are streamed to the hard disk of a SUN workstation via an ethernet connection, capable of transfer rates of 0.5 Mb s^{-1}. In practice, however, the maximum throughput of the complete system is about 0.25 Mb/s due to data handling overhead inside the PC. By storing the data on a SUN network hard disk it was possible to access them via another computer on the net, thus making it feasible to examine the acoustic measurements in real time. This opens the way to actively participating in the execution of the experiment, e.g. determine when to stop the pump in order to prevent the fracture growing out of the block.

The choice of acquisition parameters is governed by the maximum for the acoustic frequency we are concerned with, which is determined by frequency content of the waves emitted by the transducers and by the attenuation characteristics of the rock material. Results so far have shown that the effective frequency range is limited to 1250 Hz, hence a sampling rate of 2.5 MHz would suffice. However, if we want to image the fracture with an accuracy of 1 mm, then, given a maximum velocity of 5000 m s^{-1}, we need a time sampling accuracy (for imaging or first break picking) of 0.2 μs, and hence a sampling frequency of 5 MHz. This is what was chosen, with a high-pass filter of 30 kHz and a low-pass (antialias) filter of 2 MHz. Upon completion of an experiment, the raw dataset is transcribed to a SEG-Y file and stored on backup medium. Subsequent processing of the data is carried using FOCUS (CogniSeis) and SU (Colorado School of Mines).

Data description

The acquisition geometry we use to scan the model block is shown in Fig. 3. Because the transducers are placed on all six sides of the block, three different types of combination of sending and receiving transducers, or *records*, can be distinguished: diffraction records, with transducers placed on sides that are at right angles with respect to each other; transmission records, with transducers on opposite sides of the block; and reflection records, with transducers positioned on the same side of the block. These different records reveal different aspects of the fracture and will be discussed separately.

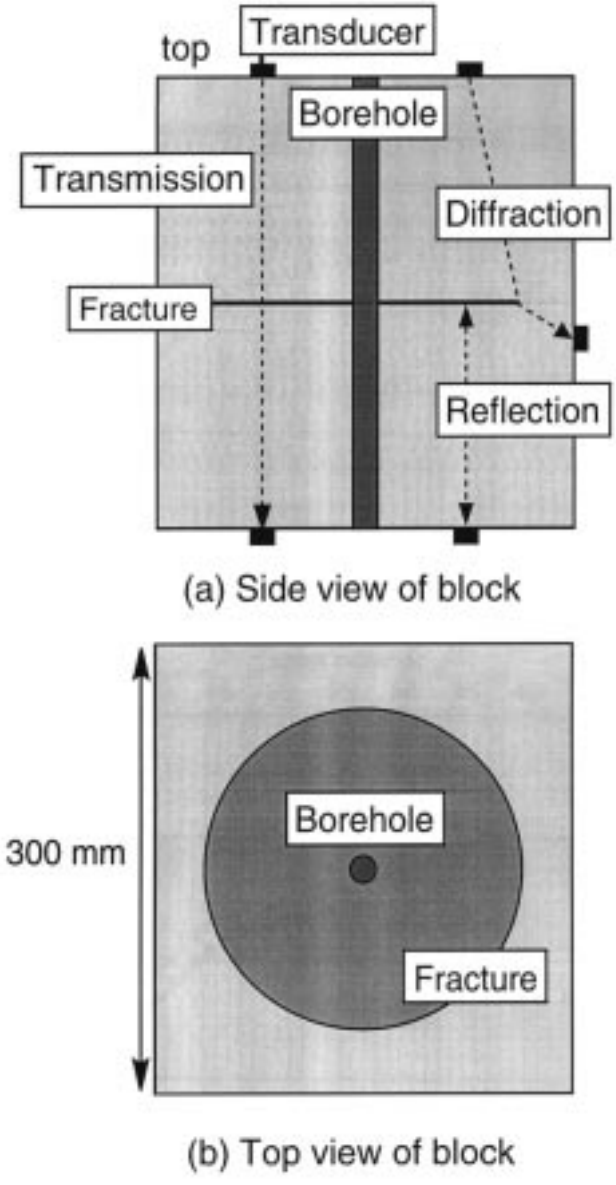

Figure 3 Schematic experimental set-up for the acoustic measurements during hydraulic fracturing tests. A horizontal fracture grows perpendicular to a vertical wellbore. The dashed lines indicate the three types of records: transmission, diffraction and reflection.

Diffraction records

The tip of the fracture appears to act strongly as a diffractor of acoustic energy. Since the fracture grows during the experiment, we observe a change in arrival time of the diffraction at later experiment time (increasing scan numbers). We can use this information to determine the position of the perimeter of the fracture during the experiment.

To use the diffraction records to their full extent, we must first process them in order to isolate the diffracted field that is caused by the growing fracture from the wealth of recorded acoustic energy. This is performed in two steps (Savic 1995). First, the incident field is removed from the measurements to obtain the total scattered field. This is accomplished by subtracting the first scan, which is recorded before the fracture is initiated, from the whole dataset. The total scattered field in turn consists of the background elastodynamic field and the field diffracted directly from the fracture. Since the background elastodynamic field does not change with time, it shows up as horizontal low frequency components in the data, which can be removed by means of a FK-filter. After this second step in the processing, we finally obtain the pure diffracted field from the tip of the fracture. See Fig. 4, which shows a diffraction record before and after processing.

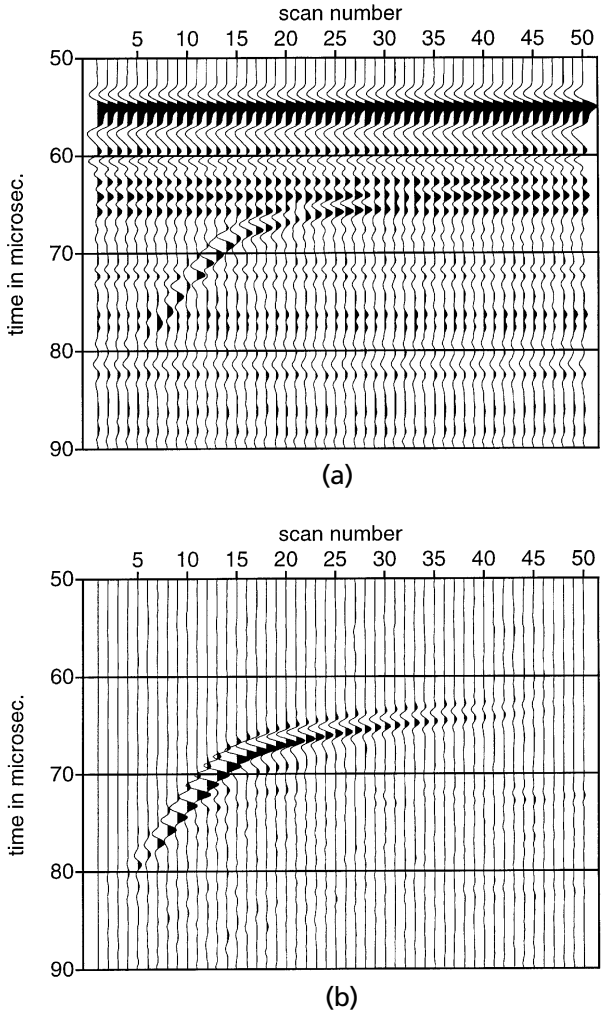

Figure 4 (a) Original diffraction record for a fixed pair of transducers, with the vertical axis denoting traveltime and horizontal axis indicating increasing experiment time. (b) Same record after processing.

Due to the large physical dimensions of the transducers, the limited number of channels and the relatively large spacing between the transducers when mounted in the loading platens, the data acquired are spatially aliased. This restricts us in the choice of migration algorithms to image the fracture. Conventional migration schemes which transform the data along the spatial axis are not suitable. We know however, the final shape of the fracture, because at the end of the experiment the block is opened and the fracture is observed and measured. Using this information, we now need only to determine the position of the fracture perimeter on the fracture surface at a given time during the experiment. This can be done by making use of the diffraction signals. The traveltime of these signals (first arrival) is strongly dependent on the fracture radius, allowing an accurate measurement of the fracture size. This requires the migration of the traveltime to the position of the diffractor. The traveltime is related to the diffractor position (or fracture perimeter) by a second order equation. In the simplest case, the fracture is radial and can be parametized with the equation of a circle. A more general approach would be to allow for an elliptic shape and parameters describing the origin and tilt of this ellipse. The number of independent measurements we have is enough to determine these parameters. The procedure is then simply to minimize the difference between observed and computed traveltime for a fracture perimeter described by a particular set of parameters. This method has been successfully applied for both radial fractures and more complex geometries. Figure 5 shows the calculated fracture radius vs. the scan number (indicating experiment time), using the first arrivals from the diffraction data of Fig. 4. In this case, where we have one radial fracture originating from the middle of the wellbore, the underlying model in the migration scheme is a circle, so one parameter (the radius) is estimated from the data. In Fig. 6 we depict a diffraction record from a fracture system consisting of multiple fracture wings, growing partly above each other. At least two clear diffraction events can be seen, each belonging to a separate fracture wing. In this more complicated case it also proved to possible to use first arrival times from diffraction records together with the *post mortem* measured geometry of the fractures to image the fracture system. Important conclusions, such as the order in which the different fracture wings were created, could thus be drawn.

Experiments on model blocks under low confining stress revealed that a weaker diffraction signal appeared before the main diffraction event. This precursor is interpreted as originating from the actual crack tip. The stronger diffraction signal arriving later originates from the fluid front. The tip of a fracture, which acts as a diffractor to acoustic waves, is in fact a somewhat complicated area, as schematically depicted in Fig. 7. It generally comprises the following elements: the front of the fracturing fluid, the nonpenetrated zone, the crack tip and a process zone in front of the crack tip. The length of the nonpenetrated zone depends on the material properties and on the stresses applied to the block in the pressure machine. In experiments with high confining stress, the nonpenetrated

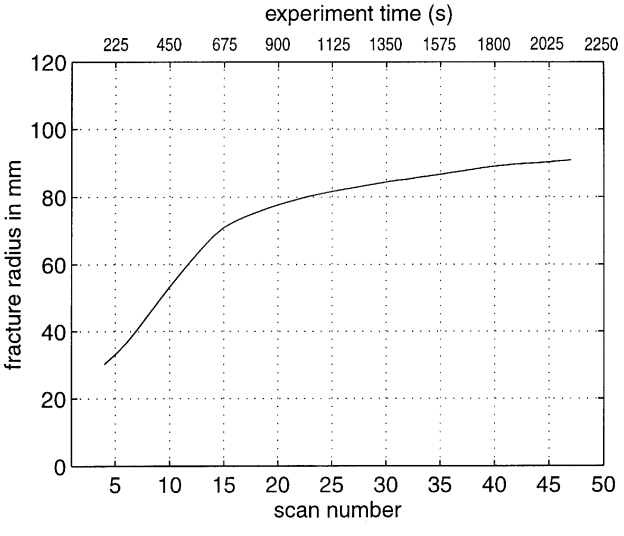

Figure 5 Radius plot using the diffraction record of Fig. 4. The vertical axis denotes the fracture radius measured from the borehole, and the horizontal axis indicates increasing experiment time.

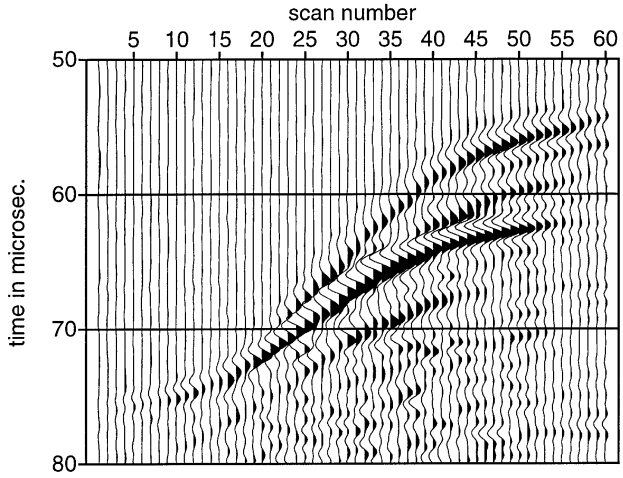

Figure 6 Diffraction record made of a hydraulic fracture system consisting of multiple fracture wings, growing partly above each other.

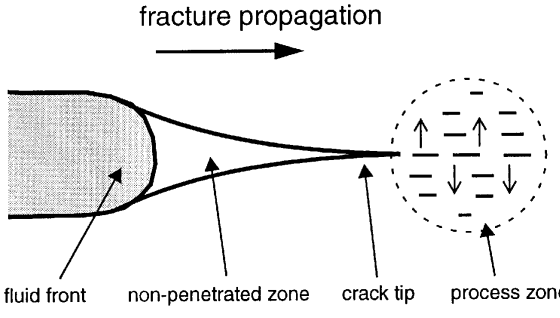

Figure 7 Simplified and schematic overview of the fracture tip area.

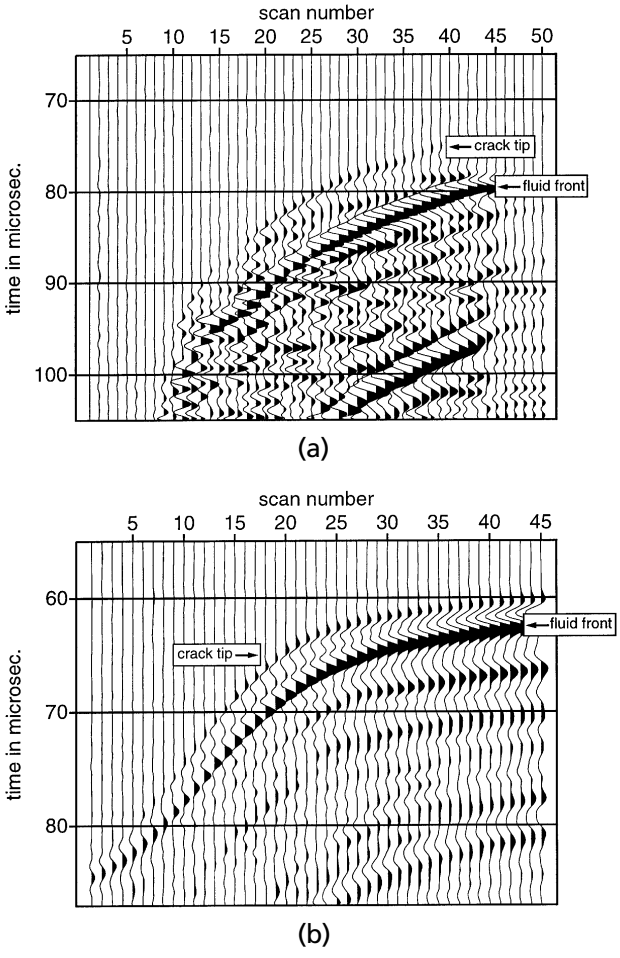

Figure 8 Diffraction record of plaster block, showing well separated diffractions of the crack tip and the fluid front. (b) Diffraction record of cement block, where the diffractions of the crack tip and the fluid front interfere.

zone is very small and the two diffraction signals coincide. In the case of low confining stress, the length of the nonpenetrated zone can be determined by the time-difference between the crack tip and fluid front diffractions.

In experiments on plaster blocks, with relatively slow P-wave velocity and large extension of the nonpenetrated zone, a clear separation of diffraction signals is observed (see Fig. 8a), making it possible to quantitatively estimate the length of the nonpenetrated zone. It is found that this length is in agreement with the actual measured length found after opening the block upon completion of the experiment. In the experiments on cement blocks under low confining stress, the crack tip is also visible in diffraction records, as seen in Fig. 8b. Because of the relatively high P-wave velocity and the smaller length of the nonpenetrated zone, the two diffractions are much closer together, but still clearly recognizable as separate events. In fact, the two signals interfere, causing subtle phase changes, which makes it difficult to obtain a good quantitative measurement. In contrast with the plaster experiments, the nonpenetrated zone diminishes slowly after shut-in and is not recognized after opening the block on completion of the experiment.

In addition to the P-wave diffractions as described above, the shear wave transducers are also able to generate diffractions from the fracture tip. This can be seen in Fig. 9, where the main shear diffraction is clearly visible between 100 and 150 μs. Although this particular record was made with both sending and receiving S-wave transducers, we can still distinguish the (much weaker) mode converted waves; from top to bottom they are the P–P wave, the S–P mode converted wave, the P–S mode converted wave and finally again the very strong S–S wave. These mode conversions mainly take place at the fracture tip, but S-wave transducers are also able to register some P-wave energy and vice versa. Analysis of the arrival times of the shear wave diffractions have shown that they are scattered from the same point on the fracture perimeter (the fracture tip), hence they also could be used to determine fracture radius by the 'migration' technique mentioned above, possibly even more accurate since the velocities are lower. In this particular picture, as often present on other records, some receding events are also seen. Shear wave transducers excite these events particularly strongly. The origin of these events is as yet uncertain, but we believe that they emanate from interactions with the wellbore. In any case, these receding events are related to the geometry of the growing fracture and we will have to spend more time and effort to unravel the complexity of these scattered events.

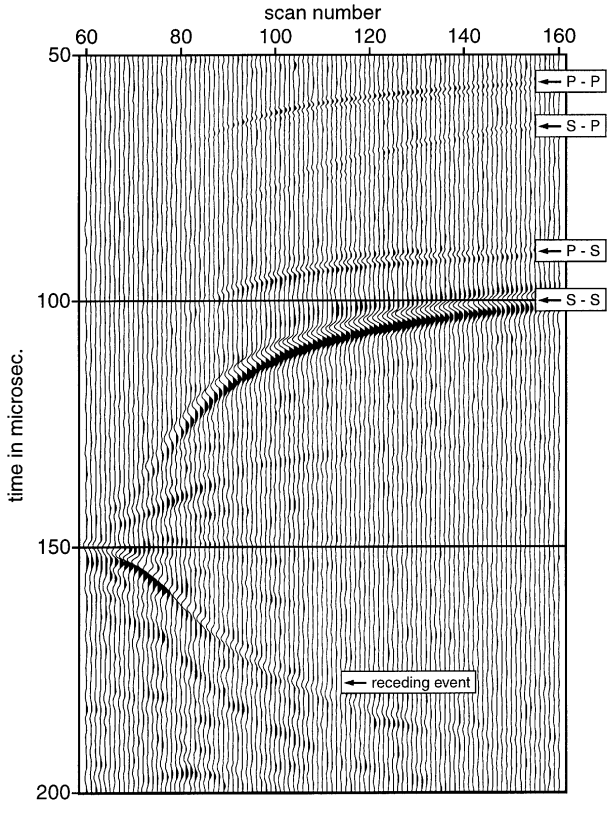

Figure 9 Diffraction record made with both sending and receiving S-wave transducers.

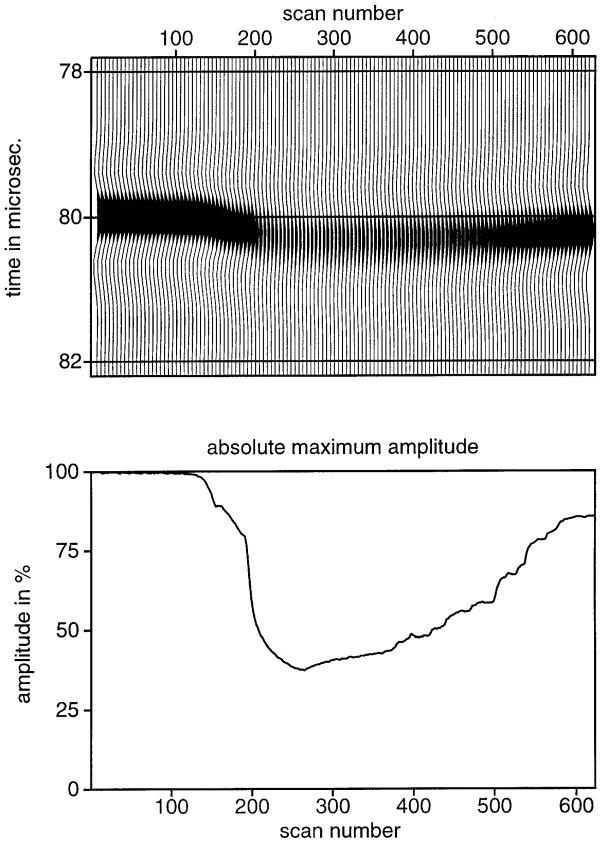

Figure 10 P-wave transmission and its amplitude curve, measured 36 mm away from the borehole. Dispersion effects caused by the growing fracture are clearly visible.

Transmission records

In addition to monitoring the *position of the tip* of the fracture using diffraction records, we would like to monitor the *width* (or opening) of hydraulic fractures during the experiment as well. We are able to measure the width of the hydraulic fracture *inside* the borehole with a LVDT, but it is also important to know the width of the fracture *away* from the borehole, since only a complete profile of the width along the fracture contains information on the pressure distribution inside the hydraulic fracture. Although the width of a fracture created inside the block is about a factor of a hundred times smaller than the wavelength of the acoustic waves scanning the block, we are still able to measure a distinct width with our ultrasonic measurements, not by a clear separation of the individual responses of the upper and lower fluid/solid boundaries of the fracture, but by a noticeable dispersion of acoustic energy in transmission records. In the case of P-waves, this dispersion shows up as an attenuation and time delay; S-wave transmissions indicate when a fracture comes into the line of sight of the transducers by exhibiting shear wave shadowing.

In Fig. 10, a transmitted P-wave, travelling from top to bottom of the model block at 36 mm radially away from the borehole, is shown. When the growing fracture crosses the line of sight of this transducer pair, around scan number 125, we observe a time delay appearing of up to 0.4 μs and an attenuation (or amplitude loss) of over 50%. After a while, the injection pump was stopped at scan number 265. From that point in time onward, the fracture is slowly closing again because the fracturing fluid leaks away into the rock and because of flow-back, decompression, etc. This corresponds to the increasing amplitude of the transmission record. At the end of the experiment, when the fracture is almost closed again, the time delay and the amplitude have recovered to their original levels. During this experiment, the width of the fracture was measured inside the borehole using a LVDT as shown in Fig. 11. Notice the distinct relationship with the amplitude profile of the transmission as shown in Fig. 10. Groenenboom & Fokkema (1997b) have provided a physical and mathematical framework to relate the observed dispersion of P-waves to the width of the fracture. Using their method we can estimate the width by comparing the original transmitted waveform (without fracture) to the dispersed waveform. The basis of this method is a 1-D convolutional model in which the theoretical signal through the fracture is related to the original signal by the transmission function of a thin layer. This transmission function effectively depends on the width, since the rock and fluid parameters necessary to calculate the transmission function remain constant and are measured separately and independently. Now for each scan, the width of the fracture can be estimated by minimizing the difference between the observed transmission response and the theoretical predicted signal, as a function of fracture.

This method has been applied to the transmission data of Fig. 10 and the estimated width profile is plotted in Fig. 11, in which the width measured at the wellbore has also been

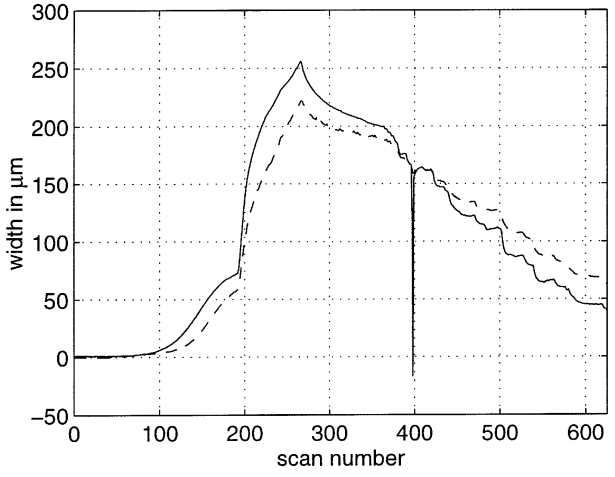

Figure 11 Width profile across the fracture, measured inside the borehole with an LVDT. (solid line) The sudden drop in width around scan number 400 is a misreading by the LVDT caused by fluid flow inside the borehole. Estimated width calculated from transmission record of Fig. 10 at a position 36 mm radially away from the borehole (dashed line).

plotted. Notice that the two curves show a remarkable agreement and that even the smallest fluctuations in the width at the wellbore are directly visible in the estimated width from the transmissions. The differences we see can be explained by realizing that the estimated width from the transmission records is 36 mm away from the borehole. As a consequence of the opening/closing mechanism of fractures, at any time during the opening phase, the fracture will be wider near the wellbore than towards the tip. After shut-in, around scan number 265, we expect the fracture to close sooner at the tip than at the wellbore. This is exactly what we observe up to scan number 360. At that point we started to pump back (extract fluid from the fracture) in order to force the fracture to close more rapidly. Then we see the width decreasing faster at the wellbore than towards the tip.

In contrast to P-waves, which travel through a fluid-filled fracture and can be used to estimate fracture width, shear waves are not able to do so, and show so called *shear wave shadowing*. In Fig. 12, we see a S-wave transmission record from the same experiment as the P-wave transmissions from Fig. 10. We now see that when the growing fracture comes in line of sight of the transducers, the amplitude of the shear wave eventually disappears. In the early part of the experiment, up to scan number 200, some diffracted energy originating from the tip of the fracture is still recorded by the transducer pair, but when the tip is sufficiently far away from the line of sight of the transducers, at which point the fracture has a width of over 75 µm, the shear wave is completely lost. At the end of the experiment, we observe that the shear wave transmission does not recover. This means that there is no physical contact between asperities on both sides of the fracture, hence the fracture is not fully closed, but some residual width exists. This is confirmed by the width profile of Fig. 11.

In experiments using a plaster block, which has a much greater leak-off than the cement block used in the experiment

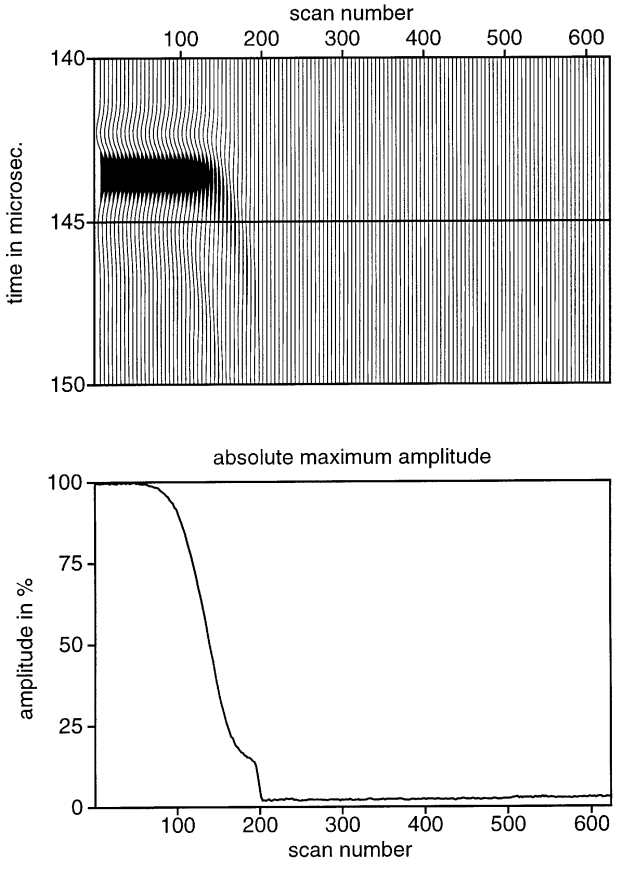

Figure 12 S-wave transmission and its amplitude curve, measured 36 mm away from the borehole. Shear wave shadowing caused by the growing fracture is clearly visible.

discussed above, the fracture is able to close completely at the end of the test, and full contact of the solid rock on both sides of the fracture is established. This effect is depicted in Fig. 13. where a S-wave transmission and its amplitude curve is plotted, and we now see the shear wave fully recovering again.

Reflection records

The last type of record to be discussed is the reflection record. There are two distinct types, generated in separate ways. First, the switchbox, as discussed earlier in the laboratory setup, can be operated to work in the pulse-echo mode. In this way, one transducer can first send out a source signal and then switch over to receiving mode to record incoming signals. This could be compared to a zero offset measurement in conventional seismics. Second, a reflection record can be generated using two transducers, one sending and the other receiving. In that case there is a certain offset associated with the record, as well as a certain midpoint, just as in conventional seismic recording.

An example of a pulse-echo reflection is shown in Fig. 14, where a P-wave reflection of the same experiment as of Figs 10–12, is plotted together with its amplitude curve. Clearly visible is the point in time where the growing fracture comes into the line of sight of the transducer around scan number 125. Reflection strength stays virtually constant between scan

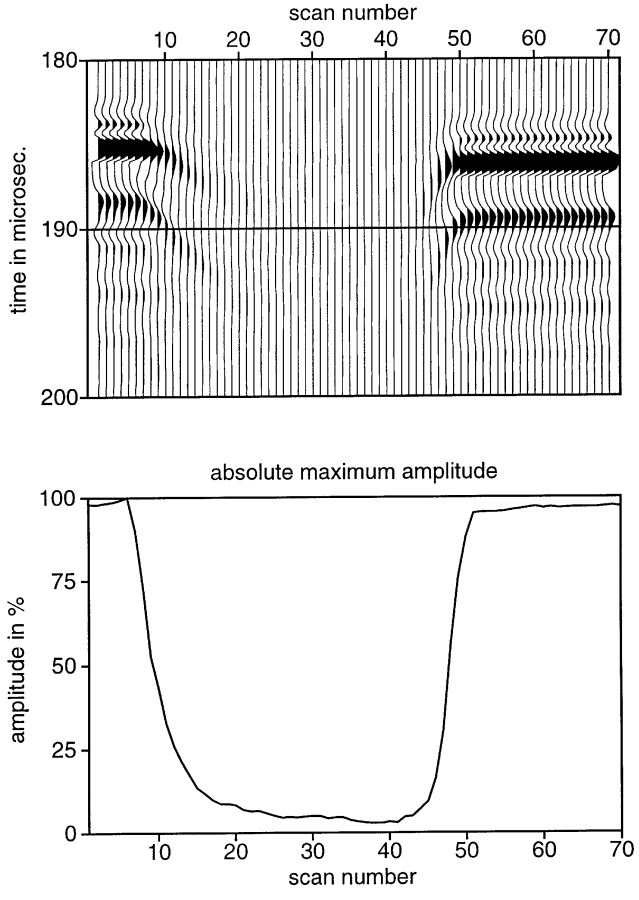

Figure 13 S-wave transmission and its amplitude curve, measured 36 mm away from the borehole. In this case the fracture closes completely at the end of the experiment and the shear wave transmission is fully restored.

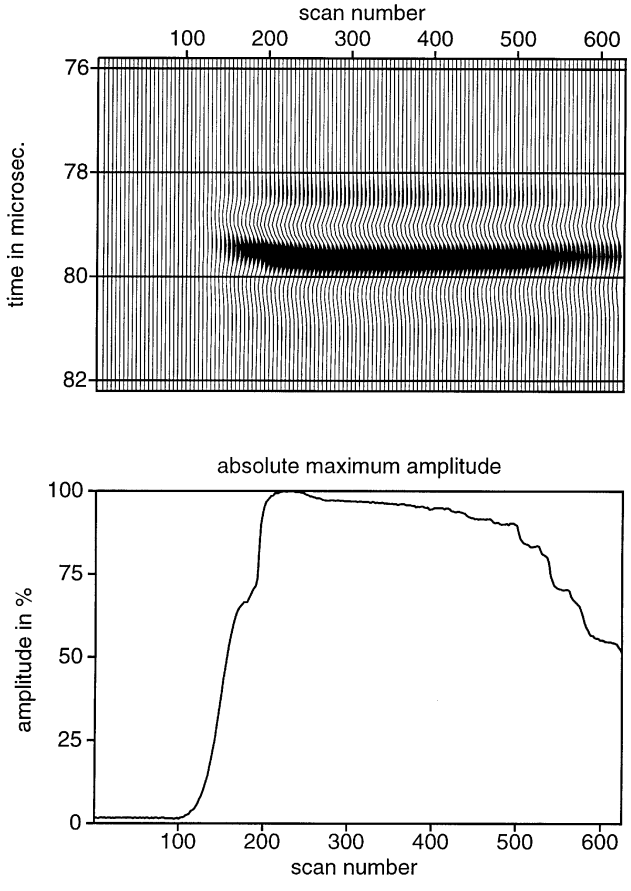

Figure 14 P-wave reflection record and its amplitude curve, measured 36 mm away from the borehole. This record is from the same experiment as Figs 10–12. When the growing fracture intercepts the line of sight of the transducer, a reflection appears.

number 200 and 500, after which it drops to 60% towards the end of the experiment. These observations are in agreement with the transmission record of Fig. 10.

Conclusions

We have succeeded in measuring ultrasonic signals scattered from a hydraulic fracture created under laboratory conditions and in using those signals to obtain information about the fracture. Diffraction records can be successfully used to image the geometrical extent of the fracture and its tip, while transmission records proved valuable to obtain a width estimate of the fracture. This last result is remarkable considering that the wavelength of the acoustic signals is many time bigger than the width of the fracture. Our method of acoustic scanning provides the possibility of using relatively low frequencies to monitor hydraulic fractures away from the wellbore. Application in field conditions may prove to be difficult because repeatability and stability of the source signal is essential. The importance of the use of shear waves is found in the resemblance with current field surveys and additional information on interaction of acoustic waves with hydraulic fractures.

Acknowledgements

This research is supported by the Dutch Technology Foundation (STW). The authors wish to thank the DelFrac Consortium, consisting of eight oil- and service companies, for supporting this project. We also thank J.T. Fokkema and C.J. de Pater for reviewing this paper. Finally we thank CogniSeis Development Inc, a subsidiary of the GeoScience Corporation, for the use of their FOCUS software package.

References

Groenenboom, J. and Fokkema, J.T. [1997b] Monitoring the width of hydraulic fractures. *Geophysics*, in press.

Groenenboom, J. and Romijn, R. [1996] Acoustic monitoring of hydraulic fracture growth, 58th Conf. & Techn. Exhib., EAGE, Extended abstracts.

Groenenboom, J., Romijn, R. and Fokkema, J.T. [1997a] Monitoring the growth of hydraulic fractures with shear waves, 59th Conf. & Techn. Exhib., EAGE, Extended abstracts.

Meadows, M.A. and Winterstein, D.F. [1994] Seismic detection of a hydraulic fracture from shear-wave VSP data at Lost Hills Field, California. *Geophysics* **59**, 11–26.

Savic, M. [1995] Ultrasonic scattering from a hydraulic fracture: theory, computation and experiment, PhD thesis, Delft University of Technology.

Weijers, L. [1995] The near-wellbore geometry of hydraulic fractures initiated from horizontal and deviated wells, PhD thesis, Delft University of Technology.

Wills, P.B., DeMartini, D.C., Vinegar, H.J., Shlyapobersky, J., Deeg, W.F.J., Woerpel, J.C., Fix, J.E., Sorrells, G.G. and Adair, R.G. [1992] Active and passive imaging of hydraulic fractures. *The Leading Edge* **11**, 15–22.

MS received April 1997, accepted May 1997